



HAL
open science

Comparative Performances of Birnessite and Cryptomelane MnO₂ as Electrode Material in Neutral Aqueous Lithium Salt for Supercapacitor Application

Aurelien Boisset, Laurence Athouel, Johan Jacquemin, Patrice Porion,
Thierry Brousse, Meriem Anouti

► To cite this version:

Aurelien Boisset, Laurence Athouel, Johan Jacquemin, Patrice Porion, Thierry Brousse, et al.. Comparative Performances of Birnessite and Cryptomelane MnO₂ as Electrode Material in Neutral Aqueous Lithium Salt for Supercapacitor Application. *Journal of Physical Chemistry C*, 2013, 117 (15), pp.7408. 10.1021/jp3118488 . hal-00961206

HAL Id: hal-00961206

<https://hal.science/hal-00961206>

Submitted on 9 May 2022

HAL is a multi-disciplinary open access archive for the deposit and dissemination of scientific research documents, whether they are published or not. The documents may come from teaching and research institutions in France or abroad, or from public or private research centers.

L'archive ouverte pluridisciplinaire **HAL**, est destinée au dépôt et à la diffusion de documents scientifiques de niveau recherche, publiés ou non, émanant des établissements d'enseignement et de recherche français ou étrangers, des laboratoires publics ou privés.

Comparative Performances of Birnessite and Cryptomelane MnO₂ as Electrode Material in Neutral Aqueous Lithium Salt for Supercapacitor Application

Aurélien Boisset,^{†,‡} Laurence Athouël,[‡] Johan Jacquemin,[§] Patrice Porion,^{||} Thierry Brousse,[‡] and Mérièm Anouti^{*,†}

[†]Laboratoire PCM2E (EA 6296), UFR Sciences et Techniques, Université de Tours, Parc de Grandmont, 37200 TOURS, France

[‡]IMN—Institut des Matériaux Jean Rouxel, Université de Nantes, UMR 6502, CNRS, 2 rue de la Houssinière, BP32229, 44322 NANTES Cedex 3, France

[§]CenTACat—School of Chemistry and Chemical Engineering, Queen's University Belfast, Belfast, Northern Ireland, U.K.

^{||}Centre de Recherche sur la Matière Divisée, CNRS—Université d'Orléans, UMR6619, 1b rue de la Férellerie, 45071 Orléans Cedex 02, France

ABSTRACT: Na-doped Birnessite-type manganese oxide (δ -MnO₂) has been synthesized using the chemical method and characterized through X-ray diffraction and SEM, showing the lamellar structure and high crystal structure. A comparative study of the electrochemical performances of this material with those of the commercial Cryptomelane-type MnO₂ has then been undertaken in ten neutral aqueous electrolytes for supercapacitor applications. Aqueous electrolytes, containing a lithium salt, LiX (where X = SO₄²⁻, N₃O⁻, C₃H₇CO₂⁻, CH₃SO₃⁻, ClO₄⁻, C₇H₁₅CO₂⁻, TFSI⁻, Beti⁻, BOB⁻, or Lact⁻), have been first prepared under neutral pH conditions to reach the salt concentration, providing the maximum in conductivity. Their transport properties are then investigated through conductivities, viscosities, and self-diffusion coefficient measurements. Second, the thermal behaviors of these electrolytic aqueous solutions are then evaluated by using a differential scanning calorimeter from (213.15 to 473.15) K in order to access their liquid range temperatures. Cyclic voltammograms (CV) in three electrode configurations are thereafter investigated using Na Birnessite and Cryptomelane as working electrode material from (-0.05 to 1.5) V versus Ag/AgCl at various sweep rates from (2 to 100) mV·s⁻¹. According to anion nature/structure and manganese oxide material type, different CV responses are observed, presenting a pure capacitive profile for Beti⁻ or C₆H₁₃CO₂⁻ and an additional pseudocapacitive signal for the smallest anions, such as ClO₄⁻ and NO₃⁻. The capacitances, energies, and efficiencies are finally calculated. These results indicate clearly that electrolytes based on a mineral lithium salt under neutral pH condition and high salt concentration (up to 5 mol·L⁻¹) have better electrochemical performances than organic ones, up to 1.4 V with good material stability and capacity retention. The relationship between transport properties, electrostatic and steric hindrance considerations of hydrated ions, and their electrochemical performances is discussed in order to understand further the lithium intercalation–deintercalation processes in the lamellar or tunnel structure of investigated MnO₂.

1. INTRODUCTION

In recent years, electrochemical supercapacitors have received considerable attention due to their ability to deliver high specific power.^{1–3} On the basis of their fundamental charge-storage mechanism, supercapacitors are categorized as electrical double-layer capacitors (EDLCs) or pseudocapacitors, which rely on fast and reversible faradic processes. Several transition metal oxides have been investigated as potential electrode materials for their uses in supercapacitors; their charge-storage mechanisms are based predominantly on pseudocapacitance.^{3,4} Manganese dioxides are considered to be potentially useful materials for pseudocapacitors not only based on their low cost, but also due to their environmental friendliness.⁵ There are several types of manganese dioxides that have [MnO₆] octahedra as the basic unit for building the Mn(IV) oxide

structure. The complexity of these different allotropic forms can be illustrated by the different nomenclature used in the literature to describe the same structure. For example, the Birnessite, which is a phyllosulfate, is characterized by a two-dimensional (2D) layered structure consisting of edge-shared MnO₆ octahedra with a basal spacing close to 7 Å. Sometimes, the Birnessite name is replaced by δ -MnO₂ or OL (octahedral layer). In same way, the Cryptomelane, which is a tectomanganate, is characterized by a 2 × 2 tunnel structure (4.6 Å side). Its name is currently replaced by α -MnO₂ or OMS-2 (octahedral molecular sieves). The Birnessite layered

structure allows high mobility of the interlayer cations with fast kinetics and little structure rearrangement that facilitates the cations intercalation–deintercalation processes,⁶ despite its specific surface being limited. *A contrario*, despite possible cation intercalation reactions in the tunneled structure, the pseudocapacitive behavior of Cryptomelane is mainly due to surface redox reactions. Such coupled pseudocapacitive mechanisms complicate the analysis and explanation of the electrochemical and physical behaviors during both charge and discharge of these manganese dioxides.⁷ But Guillemet et al.⁸ propose a physical interpretation of the charge-storage mechanism in MnO₂ through the use of a mathematical model and the determination of the physical parameters. The manganese dioxide Birnessite type has been extensively studied for its ion exchange properties, especially in the case of proton/alkali cation exchange that is related to the pH of solutions. The popularity of this material has arisen as a result of its ability to be synthesized with a relatively high surface area, and its cyclability has been tested in different aqueous salt solutions (e.g., Na₂SO₄, Li₂SO₄, or LiNO₃) in different pH conditions to investigate the impact of acidity on its stability as electrode material.⁹ However, as with many faradic charge-storage materials, their cycle life can often be limited by mechanical breakdown of the electrode as a result of repeated charge insertion/deinsertion mechanisms, as well as by solid-state phase changes due to a dissolution/precipitation mechanism. The properties of aqueous electrolytes containing an organic or a mineral lithium salt are related to the nature of the anion, which can drive the solvation properties, the mobility, and the transport properties of lithium cation in solution. In other words, the anion selection for the aqueous lithium salt electrolyte influences not only the lithium solvation pattern in the aqueous solution but also its polarizability in the material structure. Hence, the prior knowledge of transport properties, such as the viscosity, conductivity, and self-diffusion coefficients, of electrolytes provide valuable information regarding ion–ion, ion–solvent, and ion–material interactions. The link between the porosity of the electrode material and capacitance evolution has been discussed for activated carbon^{10,11} and coprecipitated MnO₂.¹² This information is, in fact, of fundamental importance for a proper understanding of the cation intercalation behavior and redox reactions into the MnO₂ structures, giving then the possibility to understand/drive/optimize the contributions from both faradic surface and faradic intercalation charge-storage mechanisms. The present study focuses on the comparative electrochemical characterization as electrode material of synthesized Na-doped Birnessite and commercial Cryptomelane in several aqueous lithium salt electrolytes. Lithium has been chosen as the cation, since it has demonstrated excellent capacitance and long-term cyclability with a Cryptomelane based electrode.⁹ In parallel, the effect of the anion structure/nature on the cycling performance in both manganese dioxides is finally investigated by taking into account different physical properties of each investigated anion, such as its size, pK_a, polarizability, and aqueous transport properties.

2. EXPERIMENTAL SECTION

2.1. Materials. All lithium salts (LiX with X = sulfate, SO₄²⁻; nitrate, NO₃⁻; perchlorate, ClO₄⁻; acetate, CH₃CO₂⁻; octanoate, C₇H₁₅CO₂⁻; lactate, Lact⁻; methylsulfonate, CH₃SO₃⁻; bis[(trifluoromethyl)sulfonyl]imide, TFSI⁻; bis-[(pentafluoroethyl)sulfonyl]imide, Beti⁻; bis(oxalato)borate,

BOB⁻) were supplied from Sigma Aldrich, with molecular purity close to 99%, and were used as received from the manufacturer. Prior to studying each aqueous LiX electrolyte, its pH was systematically controlled and adjusted using the lithium hydroxide or the corresponding HX acid to neutralize the solution (e.g., pH = 7).

Potassium persulfate (K₂S₂O₈, Labosi, molecular purity 98%), hydrated manganese sulfate (MnSO₄·H₂O, Prolabo, molecular purity 98%), and sodium hydroxide pellets (NaOH, Prolabo, molecular purity 98%) were used as received during the synthesis of the Birnessite-type MnO₂. A poly-(tetrafluoroethylene) preparation (60 wt % dispersion in EtOH, Sigma Aldrich) and Carbon Black with grade 205–110 carbon from Superior Graphite Co. were used as received as the binder and the conducting agent in the composite film, respectively.

The water was purified using a Milli-Q 18.3 MΩ water system. Commercial Cryptomelane HSSA (high surface area) was supplied and used as received from Erachem Comilog, Inc.

2.2. Methods. The X-ray diffraction patterns were measured on a Siemens D-5000 diffractometer (Bragg–Brentano configuration, Cu Kα). The materials microstructure was imaged using a Leica Stereoscan 440 and a Zeiss ULTRA plus. The surface area of each MnO₂ material was measured using a single-point BET method with a Micrometric Flowsorb II/2300 surface area analyzer using N₂ gas.

Conductivity measurements were performed by using a Crison (GLP 31) digital multifrequencies conductometer between (1000 and 5000) Hz. The temperature control ($T = 298.15$ K) was carried out within an accuracy of 0.01 K by means of a JULABO thermostatted bath. Prior to any measurement, the conductometer was first calibrated with a standard solution of known conductivity such as (0.1 and 0.01) mol·dm⁻³ KCl aqueous solutions. A TA Instrument Rheometer (AR 1000) was used to determine the viscosity of each electrolyte using a conical geometry (0.60°) at atmospheric pressure as a function of temperature from (293.15 to 373.15) K, within an operating speed of 50 rad·s⁻¹. From this study the repeatability and the uncertainty of viscosity measurements did not exceed ±0.5% and ±2%, respectively. Pulse-Gradient Spin–Echo NMR (PGSE-NMR) experiments were performed on a Bruker DSX100 spectrometer with a 2.35 T superconducting magnet, equipped with a 10 mm microimaging probe (Micro5 Bruker). The Larmor resonance frequencies ν_0 are 100.13, 39.91, and 94.22 MHz, respectively, for ¹H, ⁷Li, and ¹⁹F nuclei. A differential scanning calorimeter (Perkin-Elmer DSC 4000 under nitrogen atmosphere, coupled with an Intracooler SP VLT 100) was used to measure the thermal stability of each electrolyte. The measuring and the reference cells were filled with inert aluminum pans. Electrolytes stabilities were measured under a N₂ atmosphere with a scan rate of 2 K·min⁻¹ by using the following heating/cooling/heating rates for DSC. In each case, the sample was first cooled from (293.15 to 213.15) K, the heat flow DSC was then recorded during first a heating rate from (213.15 to 373.15) K, second a cooling rate from (373.15 to 213.15) K, and finally a heating rate from (213.15 to 473.15) K.

During this work, the same methodology as already presented by Ab Manan et al.¹³ was used to optimize each 3D structure (Gaussian version 03-D1, DFT-B3LYP-DGTZVP)^{14,15} and to generate then from this resultant optimized structure its COSMO file (TURBOMOLE, BP-DFT-Ahlich-TZVP).¹⁶ The COSMO volume and sigma

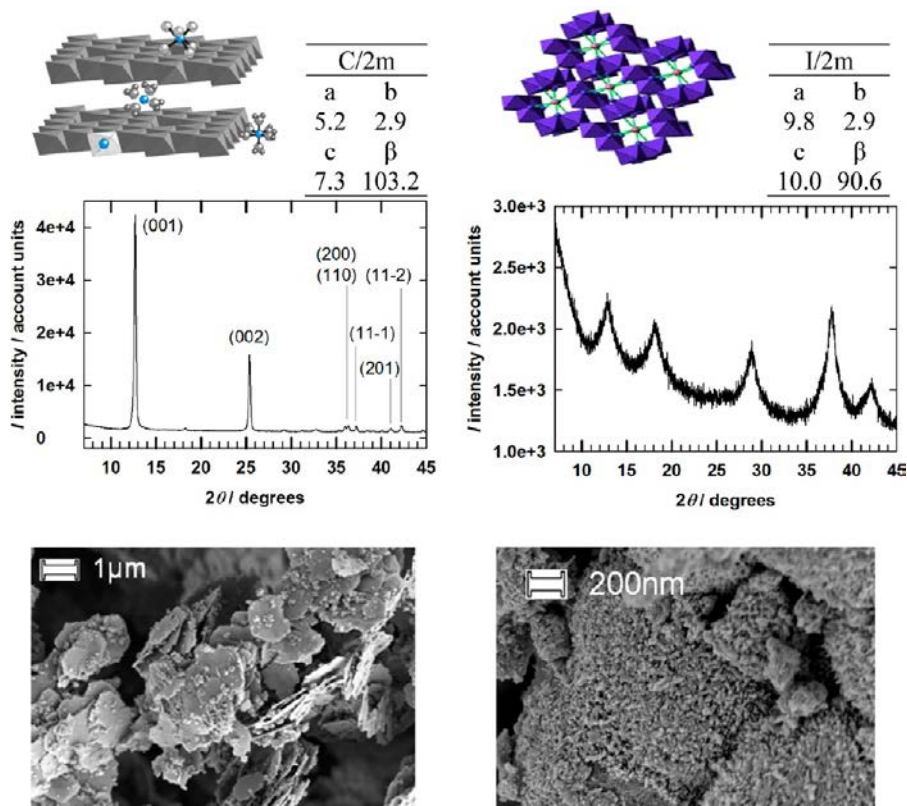


Figure 1. Crystallographic structures,²⁰ XRD patterns, and SEM analyses of respectively synthesized MnO₂ Birnessite (left) and investigated commercial Cryptomelane (right) materials (a, b, c in nm; β in degrees).

profile of each studied anion were then directly obtained by using the COSMOthermX software (version 2.1, release 01.06)¹⁷ based on the COSMO-RS (conductor-like screening model for real solvents) model.¹⁸

2.3. Synthesis of the Birnessite-Type MnO₂. Na Birnessite was synthesized according to the oxidation reaction procedure described by Ching et al.¹⁹ using pyrochroite Mn(OH)₂ and sodium persulfate Na₂S₂O₈, for which the pyrochroite was first prepared through the chemical reaction of manganese sulfate, MnSO₄·H₂O (7 mmol) dissolved into 20 mL of distilled water with an aqueous NaOH solution (6 mol·L⁻¹, 30 mL) under gentle stirring at 293.15 K. The oxidation of Mn(II) was then carried out with the addition of K₂S₂O₈ (7 mmol) powder under gentle stirring at 293.15 K. After the color variation, the mixture was then filtered, washed three times using distilled water, and dried at 333.15 K during several hours under vacuum. A brown Na Birnessite powder was finally collected and then characterized. Birnessite is a mixed oxide material that combines Mn(IV) and Mn(III) cations with Na⁺, K⁺ cations in a lamellar structure of [MnO₆] octahedra. Cryptomelane contains different manganese cations along with K⁺ in a molecular sieve-like structure of [MnO₆] octahedra. The structural characteristics of synthesized Birnessite and of commercial Cryptomelane HSSA used during this work have been studied and compared using X-ray diffractometry (XRD) and scanning electron micrographs (SEM) showing the lamellar structure and high crystal nature of Birnessite (Figure 1).

2.4. Preparation of Composite Electrodes and Electrochemical Device and Method Used. The composite electrodes were prepared according to the experimental procedure already described in the literature.^{21–23} Briefly,

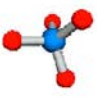
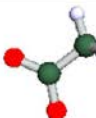
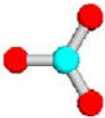
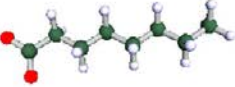
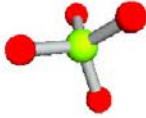
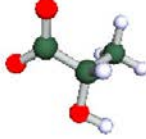

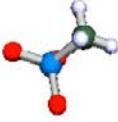

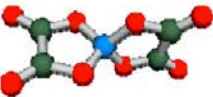
composite films were synthesized by mixing the as-prepared Birnessite (or Cryptomelane), carbon black (CB), and poly(tetrafluoroethylene) solutions within a mass ratio of 75:15:10, respectively. The mixed solution was then dispersed in ethanol using an ultrasonic bath. Ethanol was then slowly evaporated. The obtained paste was shaped into a film and dried at 333.15 K under vacuum. Material disks of diameter close to 8 mm (corresponding to around 10 mg of material) were cut and encapsulated in a stainless steel grid as current collector under 10 tons of pressure during 3 min. Note that loading corresponds to 20 mg·cm⁻², which is a standard value for carbon based electrode in commercial ECs. This allows a good comparison of capacitance, energy, and power densities, etc. values to real life devices, as mentioned by Simon and Gogotsi.¹¹


All electrochemical measurements were performed using a three electrodes cell setup using a MnO₂ disk as the working electrode, a platinum grid (2 cm × 1 cm) as the counter electrode, and an Ag/AgCl_(s) wire used as the reference electrode. The electrochemical measurements were carried out in a neutral aqueous electrolyte containing a lithium salt at 298.15 K. The cycling performance was evaluated using a Biologic Applied Research MPG2 multichannel potentiostat/galvanostat. Cyclic voltammograms (CV) were conducted at 5 mV·s⁻¹ in the voltage range from (-0.05 to 1.5) V (vs Ag/AgCl_(aq)) for at least 150 cycles and then at different scan rates of (2, 10, 20, 50 and 100) mV·s⁻¹.

3. RESULTS AND DISCUSSION

3.1. Lithium Based Neutral Aqueous Electrolytes. The lithium is the smallest in size among alkali metal cations; hence, it also has the highest charge density and polarizing power.²⁴ It

Table 1. Structure, Abbreviation, and Cosmo Volume Evaluated by CosmothermX Interface of Studied Anion (X^-) in Lithium Salt (LiX)

Structure and abbreviation	Cosmo Volume (\AA^3)	Structure and abbreviation	Cosmo Volume (\AA^3)
 SO_4^{2-}	77.7	 CH_3CO_2^-	72.1
 NO_3^-	56.7	 $\text{C}_7\text{H}_{15}\text{CO}_2^-$	202.9
 ClO_4^-	77.1	 Lact $^-$	105.4
 TFSI $^-$	219.4	 CH_3SO_3^-	92.6
 Bet i^-	299.5	 BOB $^-$	165.7



Polarisation Charge Density σ

is assumed that the solvent structural changes caused by the presence of lithium cations differ from those observed with other single-charged ions, which can apparently explain the unique and specific physicochemical properties of electrolytes based on a lithium salt solution.^{25–28} Ten lithium salts based on mineral anions (such as NO_3^- , SO_4^{2-} , ClO_4^-) and organic ones (such as TFSI $^-$, CH_3CO_2^- , CH_3SO_3^- , Bet i^- , BOB $^-$, $\text{C}_7\text{H}_{12}\text{CO}_2^-$, Lact $^-$) were selected to investigate the influence of anions' nature (organic/inorganic), size and charge density, transport and thermal properties, in order to analyze the electrochemical performances of studied materials in these electrolytes.

3.1.1. 3D Structures of Involved Ions. 3D structures, surface charge distributions, and COSMO volumes of all investigated anions are shown in Table 1. From this table, it appears that TFSI $^-$, Bet i^- , or octanoate anions have large volumes, which are up to five times higher than those calculated in the case of

the nitrate, acetate, or sulfate anions, which are the smallest anions investigated in this work. According to the surface charge distributions, as well as to the sigma profiles calculated for all studied anions (Figure 2), it appears that the charge in the Bet i^- , TFSI $^-$, and BOB $^-$ anions is highly delocalized, resulting in relatively weak cation–anion Coulombic interactions. These interactions can result in a tendency to undergo less ion association. In the case of the methylsulfonate, acetate, and octanoate anions, the presence of the alkyl chain length enhances the localization of the charge on each negative headgroup (e.g., SO_3^- or CO_2^-), but in fact, this chain length increases the van der Waals force balance in their cohesive energy (imaged by the green color in the mapped surface charge distributions). The presence of labile hydrogen on the lactate anion structure clearly has an impact on the σ profile of this molecule (blue color in the mapped surface charge

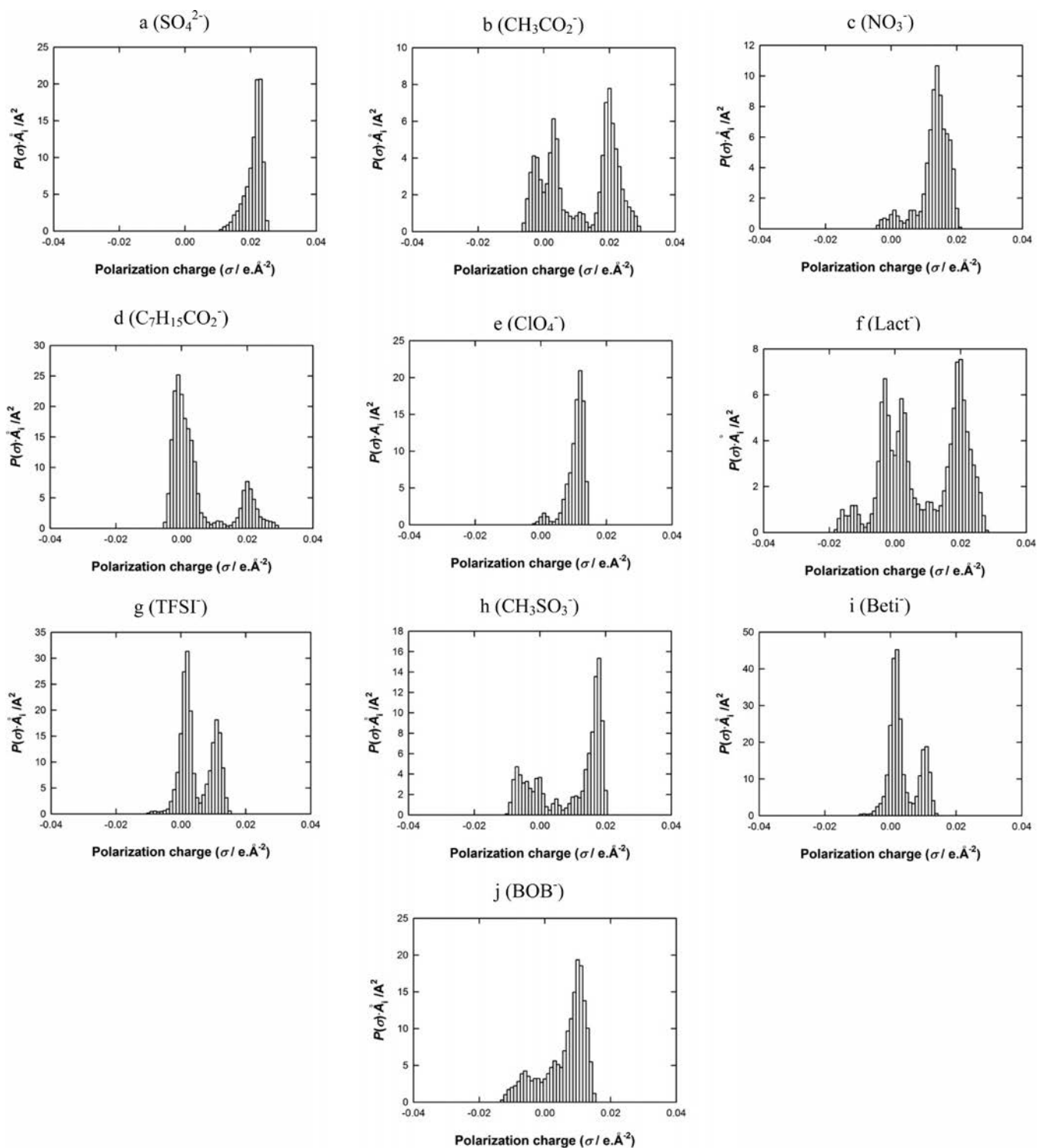


Figure 2. Sigma profiles for selected anions: a, SO_4^{2-} ; b, CH_3CO_2^- ; c, NO_3^- ; d, $\text{C}_7\text{H}_{15}\text{CO}_2^-$; e, ClO_4^- ; f, Lact^- ; g, TFSI^- ; h, CH_3SO_3^- ; i, Beti^- ; j, BOB^- .

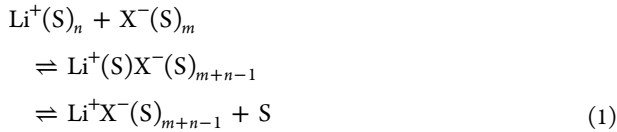
distributions). The presence of this acidic hydrogen has, in fact, an impact also on its solvation properties in water.

In the case of the symmetrical NO_3^- , SO_4^{2-} , and ClO_4^- anions, their charge densities are mainly localized on each oxygen atom. Furthermore, as their volumes are relatively small, by comparison with those obtained for the TFSI^- or Beti^- anions, strong interactions with water molecules can be imagined through different hydrogen bonds between these anions and water molecules, which, in fact, can improve their

dissociation with lithium cation. As water has very high solubility parameters, the solvation of each anion can be considered as a strong and weak base on the structure and surface charge distribution of each anion, as well as on the polarizability effect of the water molecule.

Using ab initio calculations, Dominey et al.²⁹ have estimated the intramolecular distances on the TFSI^- anion to be as follows: length = 1.45 nm and width = 0.45 nm. A similar calculation was done in the case of the ClO_4^- anion, which is a

symmetrical molecule, from which the width of this molecule is found to be close to 0.240 nm.³⁰ In fact, the observed differences in ion-pair formations between mineral salts with a small radius anion, such as LiNO₃, and large organic salts, such as LiTFSI, can be mainly attributed to the differences in their ionic radii, as well as in their surface charge distributions and σ profiles, that can reflect the charge density population on the surface of each anion. These ion-pair differences can also be analyzed by the presence of hydrogen bonding donor–acceptor sites, which can help the cation–anion dissociation in water. Nevertheless, many assumptions need to be addressed to analyze in detail the ion–pair association or dissociation in solvent; for example, we can attribute short-range forces rather than, or in addition to, insertion of a solvent molecule between the ions. These short-range forces vary as a function of solvent depending upon competing effects for ion–ion and ion–solvent interactions, and this model of the overall association process can be represented by the following:



The radius of the lithium cation is an important parameter that can impact the behavior of the cations intercalation–deintercalation processes in the 3D structure of manganese materials, and according to the literature, this radius is close to 0.8 Å.³¹ It should be noted that radii are always equal to or greater than the crystallographic radius (e.g., $\text{Li}^+_{\text{crystal}} = 0.56 \text{ \AA}$ ³²). Nevertheless, in the case of aqueous electrolytes based on (1 to 5) mol·L⁻¹ of lithium salt, the Li⁺ is mainly solvated by water molecules, generally by four molecules of solvent;³³ then, depending of the nature of the anion, different complexes can be imagined. In the case of organic anions (such as LiBetI, LiTFSI, etc.), it is possible to consider that the most favorable complex in water is the contact ion pair: that is, the last complex in eq 1 ($\text{Li}^+\text{X}^-(\text{S})_{m+n-1}$), which may still be a solvated species. In the case of the electrolytes based on small mineral anions (LiNO₃, Li₂SO₄, and LiClO₄), according to the above discussions (Table 1 and Figure 2), the most favorable complex can be the first representation in eq 1, i.e. $\text{Li}^+(\text{S})_n + \text{X}^-(\text{S})_m$. Therefore, according to eq 1, this model assumes that, upon association, the anion displaces a solvent molecule from the solvation sphere of the lithium cation. These considerations will be discussed with respect to the lithium insertion mechanism into the Birnessite or Cryptomelane structure.

3.1.2. Conductivities of Lithium Salt Aqueous Electrolytes.

The origin of the exceptionally high solubility of anhydrous lithium salt in organic or in aqueous solvents has been a matter of some conjecture.³⁴ The combination of small cation with a large anion must induce favorable balance of lattice and solvation energies conducive to extensive solubility in a wide range of solvents.³⁴ The solubility and stability of lithium salts have prompted their use as solute in electrolytes for supercapacitors. While several studies concern the use of aqueous solutions of LiNO₃ and Li₂SO₄ as electrolytes for supercapacitors, few works concern lithium salts with organic anions. Figure 3 shows ionic conductivities at 25 °C of ten aqueous solutions containing a different lithium salt as a function of the salt concentration. In general, the ionic conductivity of an electrolyte solution passes through a maximum by increasing electrolyte salt concentration. For

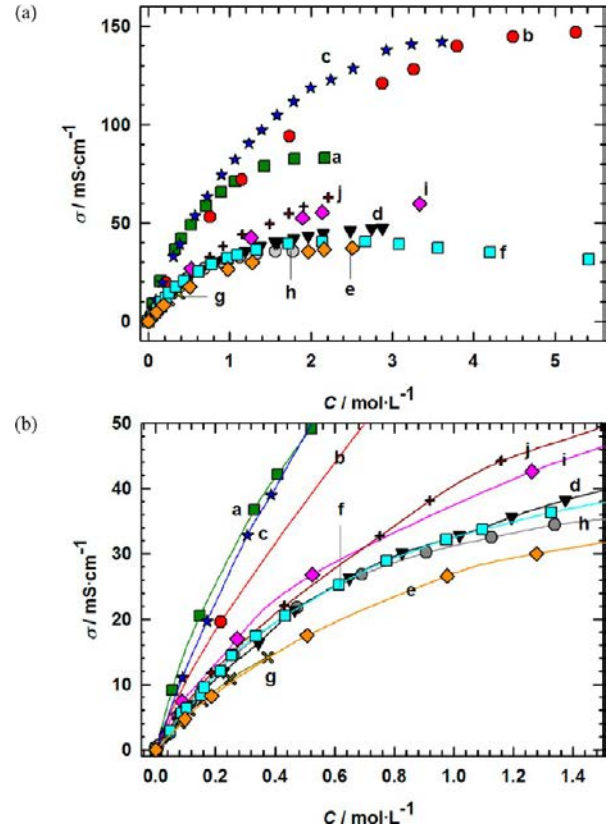


Figure 3. Evolution of the conductivity, σ , as a function of the molar concentration of aqueous solution of lithium salt at 25 °C (a) and a zoom at low molar concentration (b): a, green squares, SO_4^{2-} ; b, red circles, NO_3^- ; c, black stars, ClO_4^- ; d, \blacktriangledown , TFSI⁻; e, orange diamonds, BetI^- ; f, light blue squares, CH_3CO_2^- ; g, yellow \times , $\text{C}_7\text{H}_{15}\text{CO}_2^-$; h, gray circles, Lact^- ; i, magenta diamonds, CH_3SO_3^- ; j, brown plus signs, BOB^- .

low salt concentrations, the conductivity increase is due to an increase in the number of charge carriers. By increasing the salt concentration, both ionic association and viscosity increase in the solutions, which take place mainly due to enhancement of the ion–ion interaction. We can classify studied salts based on their solubility in water. NO_3^- and Ac^- anions have a higher solubility in water ($C > 5 \text{ mol}\cdot\text{L}^{-1}$) than lactate and octanoate ones, which are the lesser water-soluble salts studied herein ($C < 2 \text{ mol}\cdot\text{L}^{-1}$). All other salts studied during this work have solubility in water between these two concentration limits. Each maximum concentration of salt reported in Figure 3 does not correspond necessarily to the limit of solubility, since when the salt is sufficiently soluble, we stopped to add it in the electrolyte for concentrations beyond the maximum of conductivity, C_{cycling} . Indeed, the lithium salts based on the nitrate, methanesulfonate, and sulfate anions are described to have a solubility in water close to (5.3, 3.02, and 7.06) mol·L⁻¹, respectively.^{35,36} Furthermore, it can be noted also that the LiNO₃, LiAc, which are the most soluble in water, have also the lowest Cosmo volumes (Table 1), while those having the highest conductivity in aqueous solution are those presenting a charge density highly localized on the anion, i.e. SO_4^{2-} , NO_3^- .

From Figure 3 it can also be pointed out that only sulfate, nitrate, and chlorate based salts have higher conductivities than tetraethylammonium tetrafluoroborate in acetonitrile, which is the standard electrolyte in commercial EDLCs.

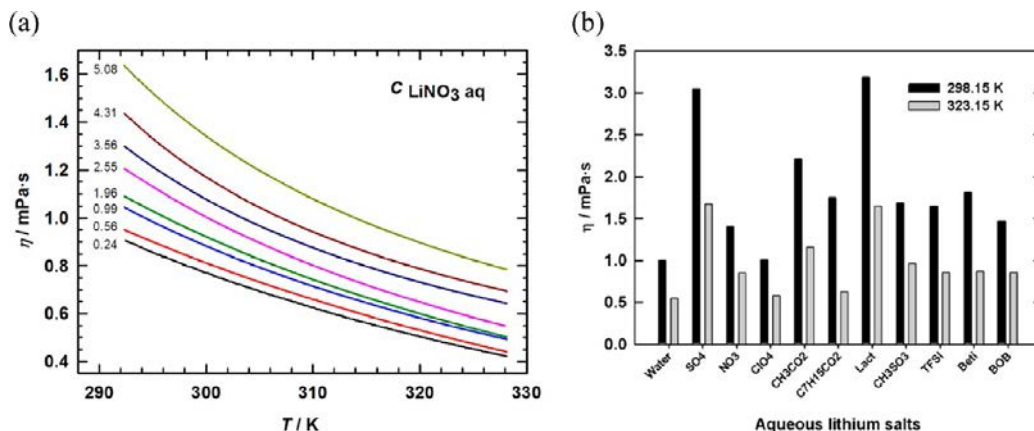


Figure 4. Variation of viscosities as a function of temperature of aqueous solutions (a) LiNO_3 at various compositions (numbers provided to the left of each curve in $\text{mol}\cdot\text{L}^{-1}$) and (b) different aqueous lithium salt solutions at their optimal concentrations, C_{cycling} .

Table 2. Transport Properties (σ Ionic Conductivity and η Viscosity) and $\Lambda\cdot\eta$ Walden's Product in Aqueous Lithium Salts at $1.0 \text{ mol}\cdot\text{L}^{-1}$ (Concentration in Lithium Cation at 298 K) and Transport Properties at Cycling Concentrations in Salt at 293 K

lithium salt $C_{\text{Li}^+} = 1.0 \text{ mol}\cdot\text{L}^{-1}$	σ ($\text{mS}\cdot\text{cm}^{-3}$)	η ($\text{mPa}\cdot\text{s}^{-1}$)	$\Lambda\cdot\eta$	C_{cycling} ($\text{mol}\cdot\text{L}^{-1}$)	σ_{cycling} ($\text{mS}\cdot\text{cm}^{-1}$)	η_{cycling} ($\text{mPa}\cdot\text{s}$)
Li_2SO_4	47.8	0.976	46.7	2	83.1	2.57
LiNO_3	64.9	0.883	57.3	5	146.9	1.53
LiClO_4	87.1	0.849	73.9	1.8	111.7	1.02
LiCH_3CO_2	32.6	1.209	39.4	2.5	40.5	2.32
$\text{LiC}_7\text{H}_{12}\text{CO}_2$				0.5	14.2	2.43
LiLact	31.2	1.233	38.5	1.8	35.5	2.35
LiCH_3SO_3	37	1.023	37.9	3.4	59.7	1.93
LiTFSI	32.5	1.165	37.9	2.5	46.1	2.21
LiBetI	26.6	1.611	42.9	1	26.6	1.8
LiBob	40.1	1.148	46	2.2	62.9	1.73

3.1.3. Viscosities of Lithium Salt Aqueous Electrolytes. The ion mobility is directly related to the viscosity of solutions, which reflects the interaction forces solvent–solvent and solvent–ion. The change in viscosity caused by the addition of a salt is roughly proportional to the concentration at low concentrations but increases more rapidly than the concentration at high concentrations. For studied electrolytes, viscosity variations were measured as a function of concentrations from 0 to C_{cycling} , as shown in Figure 4a in the case of LiNO_3 . Table 2 reports the comparative values of viscosities, conductivities, and Walden's product ($\Lambda\cdot\eta$) at same concentration ($C = 1 \text{ mol}\cdot\text{L}^{-1}$) for selected aqueous solutions, from which it appears that all viscosity values are higher than the viscosity of pure water ($\eta = 0.89 \text{ mPa}\cdot\text{s}$ at 25°C). From Table 2, we note also that LiNO_3 and LiClO_4 present higher Walden's products, up to 73.9 and 57.3, respectively, than other studied electrolytes. In other words, LiNO_3 and LiClO_4 aqueous solutions are the most ionic electrolytes.

Figure 4b shows the comparative viscosity solutions at 298 and 323 K. From this figure it appears that the solutions based on lactate and sulfate anions have the highest viscosity values, while ClO_4^- presents the lowest ones, which are close to the viscosity values of water. During the cyclability tests using manganese oxide electrodes, we decided to work with a lithium salt concentration, which provides the optimal transport properties: i.e. at maximum on conductivity and minimum on viscosity in the different investigated electrolytes. Such values are reported in Table 2 at 20°C , where C_{cycling} represents this optimal salt concentration for each aqueous solution.

3.1.4. Self-diffusion by Pulse-Gradient Spin–Echo NMR (PGSE-NMR). The PGSE-NMR method is used to measure the self-diffusion of a variety of ionic species.^{37,38} In the present study, for each of two model electrolytes (Li_2SO_4 $2 \text{ mol}\cdot\text{L}^{-1}$ and TFSI $2.5 \text{ mol}\cdot\text{L}^{-1}$), solvent (H_2O molecules) and cationic and anionic self-diffusion coefficients were determined by proton (^1H), lithium (^7Li), and fluorine (^{19}F) NMR experiments, respectively. To improve the accuracy of the self-diffusion coefficients measurements, a modified stimulated spin–echo sequence was utilized.³⁹ It consists in a 13-interval PGSTE pulse sequence⁴⁰ with a bipolar-gradient pair (see Figure 5). By using the PGSE-NMR method, self-diffusion coefficients were determined by measuring the decrease of the NMR echo signal intensity through increasing magnetic field gradients (g). The self-diffusion coefficients, D , were then obtained by a simple linear least-squares fitting of the classic echo attenuation relationship according to the following:

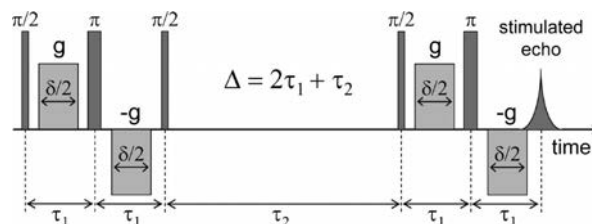


Figure 5. Schematic view of the 13-interval PGSTE-NMR pulse sequence. This NMR sequence produced a stimulated spin–echo at the time $t = 4\tau_1 + \tau_2$. The diffusion time is defined by $\Delta = 2\tau_1 + \tau_2$.

$$E(g, \Delta) = I(g, \Delta)/I(0, \Delta) = \exp[-\gamma^2 g^2 \delta^2 D(\Delta - \delta/3)] \quad (2)$$

where $I(g, \Delta)$ and $I(0, \Delta)$ are the echo intensities, respectively, measured with and without the field gradient g (varying between 0 and g_{\max}), respectively. δ is its duration, γ is the gyromagnetic ratio of the nuclei, Δ is the diffusion time (fixed to 50 ms), and D is the self-diffusion coefficient.

Depending on the electrolyte sample and the NMR nuclei, the magnetic field gradient duration δ was varied between 1 and 3 ms, and the recovery delay was ranged from 6 to 40 s. In addition, the maximum value of the magnetic field gradient (g_{\max}) was set to 1.6 T/m and the temperature was regulated at 290 K.

The obtained values (Table 3) indicate that the mobility of the lithium cation is higher (45% more important) in LiTFSI

Table 3. Comparative Relative Diffusion of Water Molecules and Lithium Cation in Two Aqueous Lithium Salts at 2.0 mol·L⁻¹

Li ₂ SO ₄	LiTFSI
$D_{\text{IH}} = D_{\text{H}_2\text{O}} = 6.5 \times 10^{-10} \text{ m}^2/\text{s}$	$D_{\text{IH}} = D_{\text{H}_2\text{O}} = 9.2 \times 10^{-10} \text{ m}^2/\text{s}$
$D_{7\text{Li}} = D_{\text{Li}^+} = 2.9 \times 10^{-10} \text{ m}^2/\text{s}$	$D_{7\text{Li}} = D_{\text{Li}^+} = 4.2 \times 10^{-10} \text{ m}^2/\text{s}$
	$D_{19\text{F}} = D_{\text{TFSI}} = 2.9 \times 10^{-10} \text{ m}^2/\text{s}$
$\frac{D_{\text{H}_2\text{O}}^0}{D_{\text{H}_2\text{O}}} = \frac{1.9 \times 10^{-9}}{0.65 \times 10^{-9}} \approx 2.92$	$\frac{D_{\text{H}_2\text{O}}^0}{D_{\text{H}_2\text{O}}} = \frac{1.9 \times 10^{-9}}{0.92 \times 10^{-9}} \approx 2.07$
$\frac{D_{\text{Li}^+}^0}{D_{\text{Li}^+}} = \frac{9 \times 10^{-10}}{2.9 \times 10^{-10}} \approx 3.10$	$\frac{D_{\text{Li}^+}^0}{D_{\text{Li}^+}} = \frac{9 \times 10^{-10}}{4.2 \times 10^{-10}} \approx 2.14$
$x = \frac{D_{\text{H}_2\text{O}}^0 - D_{\text{H}_2\text{O}}}{D_{\text{H}_2\text{O}}^0 - D_{\text{Li}^+}} = 0.78$	$x = \frac{D_{\text{H}_2\text{O}}^0 - D_{\text{H}_2\text{O}}}{D_{\text{H}_2\text{O}}^0 - D_{\text{Li}^+}} = 0.66$
78% of solvating water moles	66% of solvating water moles
22% of free water moles	34% of free water moles

electrolyte solution than that for the Li₂SO₄, signifying that TFSI⁻ anion is less “attached” to the lithium cation. The comparative relative diffusion of water molecules and lithium cation is summarized in Table 3. These results show that, in the case of organic salt, there is a greater proportion of free water molecules. The nature of free or solvating water will explain their participation in pseudocapacitive redox processes discussed in the next paragraph.

3.1.5. Thermal Properties. The thermal behavior of the studied electrolytes was investigated by DSC from -60 to 200 °C. Figure 6 presents a thermogram recorded at a scan rate of 5 °C·min⁻¹ during heating from -20 to 200 °C (step I) followed by cooling from 200 °C to -60 °C (step II) in the case of aqueous Li₂SO₄ 2 mol·L⁻¹ solution. This thermogram shows the crystallization phase transitions observed at $T_c = -37.9$ °C ($\Delta H_c = -87.0 \text{ J}\cdot\text{mol}^{-1}$) and a characteristic peak for the eutectic mixture of water + Li₂SO₄, corresponding to gradual fusion of the mixture. In this present example, the boiling temperature of the aqueous Li₂SO₄ 2 mol·L⁻¹ solution is observed at 150 °C. A similar experimental methodology was then followed for each investigated electrolyte. From each recorded DSC thermogram, it is then possible to calculate for each studied electrolyte their crystallization, ΔH_c , and melting, ΔH_m , enthalpy values (reported in Table 4). In the case of LiClO₄ and LiNO₃ aqueous solutions, ΔH_m values are close to

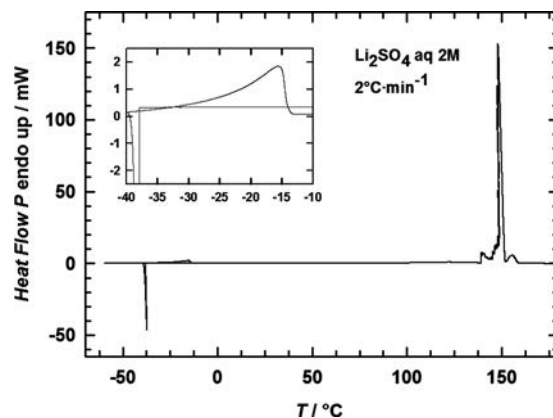


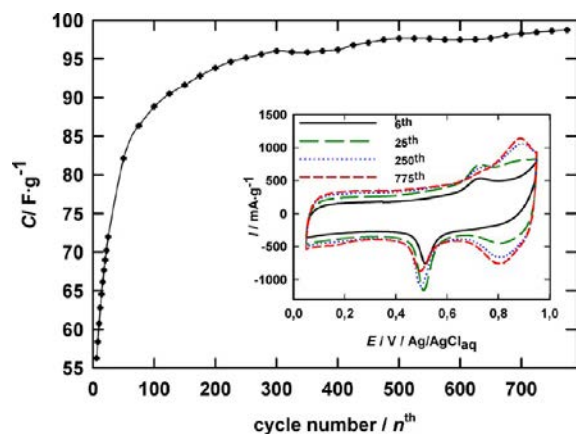
Figure 6. DSC thermogram showing different phase transitions of aqueous 2 M Li₂SO₄.

378.7 J·mol⁻¹ and 211.2 J·mol⁻¹, respectively, which indicates, as expected, that these salts are more hydrated by water than the LiTFSI one. All investigated electrolytes have a large liquid (and stability) range; for example, in the case of the aqueous lithium sulfate electrolyte, this range is between -15 and 130 °C. This temperature range is not an issue for this work, since our target is to test the performance of the aqueous electrolyte containing a lithium salt at room temperature. Furthermore, it can be noted that unlike acetonitrile based electrolytes used in commercial EDLCs, all investigated aqueous based electrolytes have a quite “high” boiling point, which is quite interesting for safe operation of the MnO₂ based cells at fast current densities.⁴¹ However, for low temperature applications (below -20 °C), only LiNO₃ and LiTFSI salts can be suitable.

3.2. Electrochemical Performance. To characterize the elaborated MnO₂ electrode, we have measured, in a small volume (15 mL), with three electrode cell, cyclic voltammograms of Birnessite in 5 M LiNO₃ at the scan rate $\nu = 5 \text{ mV}\cdot\text{s}^{-1}$ from -0.05 to 0.9 V vs Ag/AgCl(s). Figure 7 shows the CV curves for the prepared Birnessite at 5 mV·s⁻¹ where the current has been translated into the specific capacitance per unit mass of electroactive material. The shape of the obtained curve is different from the classical rectangular curve observed in the case of capacitive phenomena. The rectangular shape envelope witnesses a pseudocapacitive charge-storage mechanism arising from fast, reversible faradic reaction, probably located at the surface of the material. The superimposed redox peaks are related to partial intercalation of cations in the lamellar structure, as demonstrated.²² We note that the capacitance evolved rapidly during the first cycles to reach a stable value after 300 cycles, indicating the progressive wettability of electrode in this electrolyte, and then this value remained stable up to 700 cycles. Birnessite-type MnO₂ with lamellar structure can facilitate the lithium intercalation-desintercalation with the increase of interlayer spacing.⁴² In addition, there are two cathodic peaks at (0.5 and 0.8) V vs Ag/AgCl(s) and a reverse anodic peak at (0.7 and 0.85) V vs Ag/AgCl(s). These peaks suggest that there are two different processes of cation intercalation. This suggestion is well in agreement with possible intercalation sites in Birnessite. Different charge environments in these sites involve different conditions (such as voltage tension) to access and stay in each type of site. These superimposed redox peaks can be compared as pure intercalation peaks occurring in classical battery electrode charge/discharge cycles of classical battery electro-

Table 4. Thermal Properties of Selected Aqueous Electrolytes Containing a Lithium Salt

lithium salt	T_c (°C)	T_m (°C)	T_b (°C)	ΔH_c (J·mol ⁻¹)	ΔH_m (J·mol ⁻¹)
2 M Li ₂ SO ₄	-37.9	-15.6	139.1	-87.0	86.8
5 M LiNO ₃	-50.4	-23.9	140.8	-208.3	211.2
2.5 M LiTFSI	-46.7; -10.7	-42.1	125.1-139.9	-5.2	25.5
				-11.3	
1.8 M LiClO ₄	-52.5; -24.5	-14.9 to 8.6	125.6	-87.2	378.7
				-151.5	


Figure 7. Electrochemical response of a MnO₂ Birnessite electrode in 5 M LiNO₃, CV of MnO₂ (in inset) and capacitance as a function of cycle number.

des.⁴³ Moreover, dissymmetry between superimposed anodic and cathodic peaks during the scan indicates that the mechanism is not easily reversible.

In order to compare the capacitive response of Birnessite- and Cryptomelane-type MnO₂ materials, we operated under the same conditions as those described above, after assuring the wettability of electrodes was fully achieved. The stable electrochemically active potential window was evaluated between (-0.05 and 1.35) V vs Ag/AgCl(aq). Figure 8 shows electrochemical responses of MnO₂ as a function of the width of the active potential window. Usually the electrochemical window is limited to 0.95 V in aqueous media, due to instability of MnO₂ in non-neutral aqueous solution. But for our materials and electrolytes, it seems possible to charge and discharge electrode material at higher potential up to 1.4 V vs Ag/AgCl(aq). CV obtained in LiNO₃, LiTFSI, Li₂SO₄, and LiClO₄ illustrates the predominance of surface pseudocapacitive phenomena in the case of Cryptomelane. Indeed, the intercalation of cations is also present, as illustrated by the presence of two reversible broad peaks centered at 0.6 and 1.1 V in oxidation (vs Ag/AgCl). The superimposed redox peaks are more pronounced for Birnessite than for Cryptomelane, especially for mineral anion. This observation is in agreement with their structural differences. The experimental capacitance, after the subtraction of the influence of acetylene black, is, respectively, close to 150 F·g⁻¹ for the Birnessite and 180 F·g⁻¹ for the Cryptomelane. These values are in agreement with capacitance data available in the literature for the same materials.⁴⁴ The capacitance retention ratio as a function of the cycles number at (0.9 and 1.4) V for all studied electrolytes is presented in Table 5. To our best knowledge, few studies relate a wide cycling with satisfactory stability for 300 cycles without drastic capacitance loss, as shown in Table 5.

The influence of the nature of salts on observed electrochemical behavior is notable in Figure 8. As in the case of the 5 M LiNO₃ electrolyte, the stability of the Birnessite-type MnO₂ supports a voltage window of 1.4 V (Figure 8b₂); in the case of lithium acetate, stability is limited to 1.1 V (Figure 8b₄). This feature can be explained by the basicity of the organic anion, which impacts the localized proton availability inside the material structure. There is even in the case of LiBetri an extension of the potential window up to 1.6 V (Figure 8b₆). In addition, we note a disappearance of the superimposed redox peaks in the case of LiBetri, indicating an absence of redox exchange of Li⁺ into the lamellar structure of Birnessite.

To understand the relationship between the observed electrochemical oxidation stability and the nature of the selected anion, the potential limits defined by the onset of the limit current of oxidation of each electrolyte solution were correlated as a function of the anion (denoted X⁻) basicity expressed by its pK_a (HX/X⁻). It appears from Figure 9 that the basicity of the anion X⁻ seems to be a key parameter in the redox behavior of salt toward the Birnessite. This can be easily explained by considering that the surface redox reaction mechanism in MnO₂ material involves a proton (as expected from eq 1). We also note in Figure 9 that the lactate anion has an atypical behavior, since this salt does not follow the correlation as observed for the other ones. This is probably due to the presence of the alcohol group on its structure, which can potentially provide a labile proton, as depicted from its σ profile (see Table 1). On the other hand, when the anion derives from a hyperacid as lithium salts containing TFSI⁻, BOB⁻, and Betri⁻ (pK_a close to -40), the neutral character of the anion cannot be differentiated, as for example in the case of the ClO₄⁻ (pK_a = -7) based electrolyte. From our investigation, for pK_a lower than -7, the potential limit on Birnessite material seems to no longer depend on the nature/structure of the electrolyte, but only on the vulnerability of the material to the oxidation. For Birnessite-type MnO₂, this limit is estimated to be close to 1.6 V.

On the other hand, the size of the ions is potentially another key parameter of the electrochemical properties of Birnessite materials. Such a correlation (Figure 10) was realized by using current of cathodic peak (ip^c) values in the case of the Birnessite in each investigated electrolyte, as well as the COSMO volumes (Table 1) of each individual anion. As shown in Figure 10, it appears that the volume of the anion is, as the pK_a, a key parameter able to correlate the pseudocapacitive behavior of the Birnessite material. As shown in this figure, larger anions inhibit the insertion; consequently, the i(ep^c) decreases and tends to zero for the larger ones, such as Betri⁻ or the octanoate. It also appears from this curve that the correlation between these two properties ends for any anion presenting a COSMO volume lower than 71 Å³ or, in other words, a diameter close to 7 Å. As this distance corresponds to the space between the lamellar layer of Birnessite, it appears

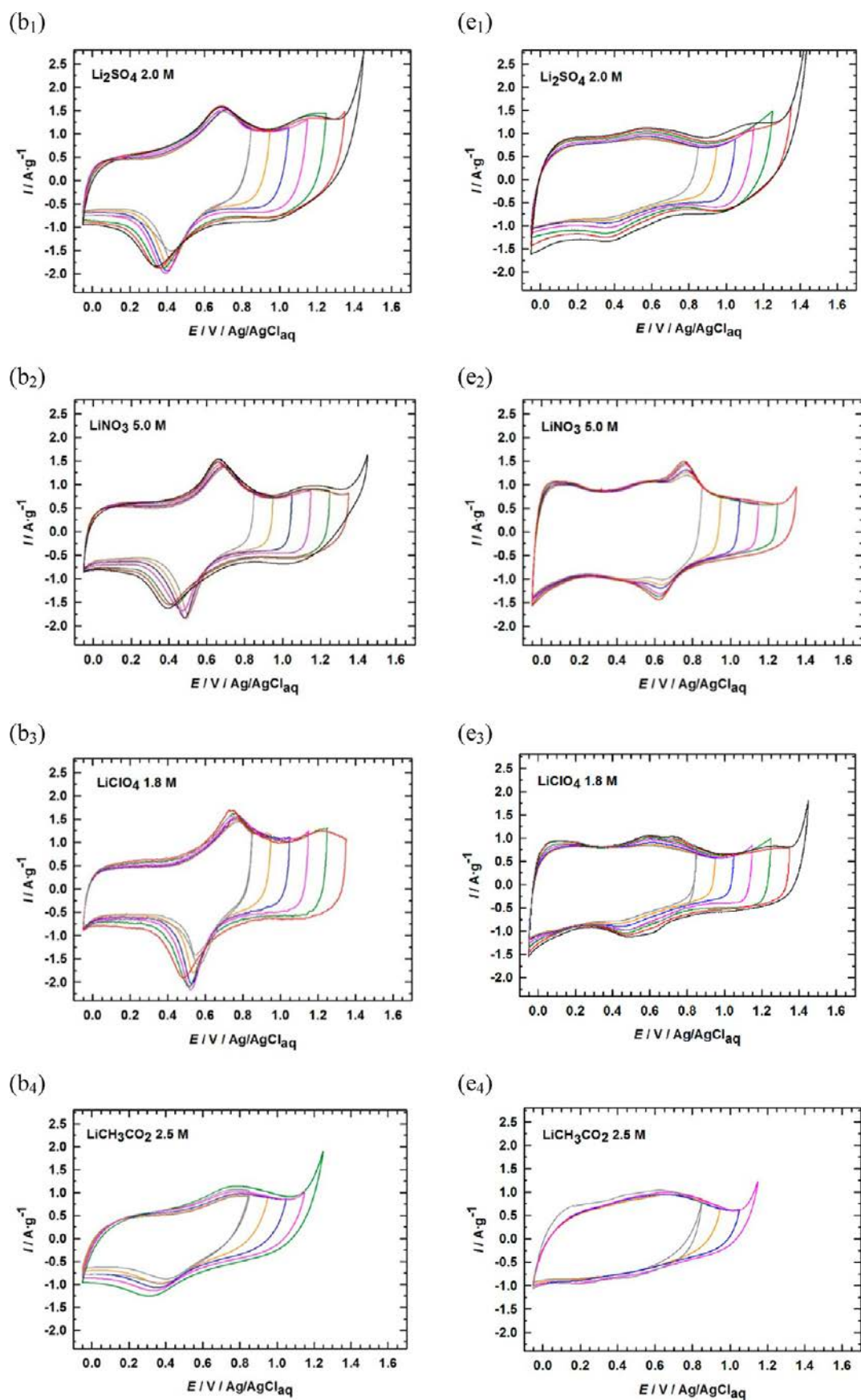


Figure 8. continued

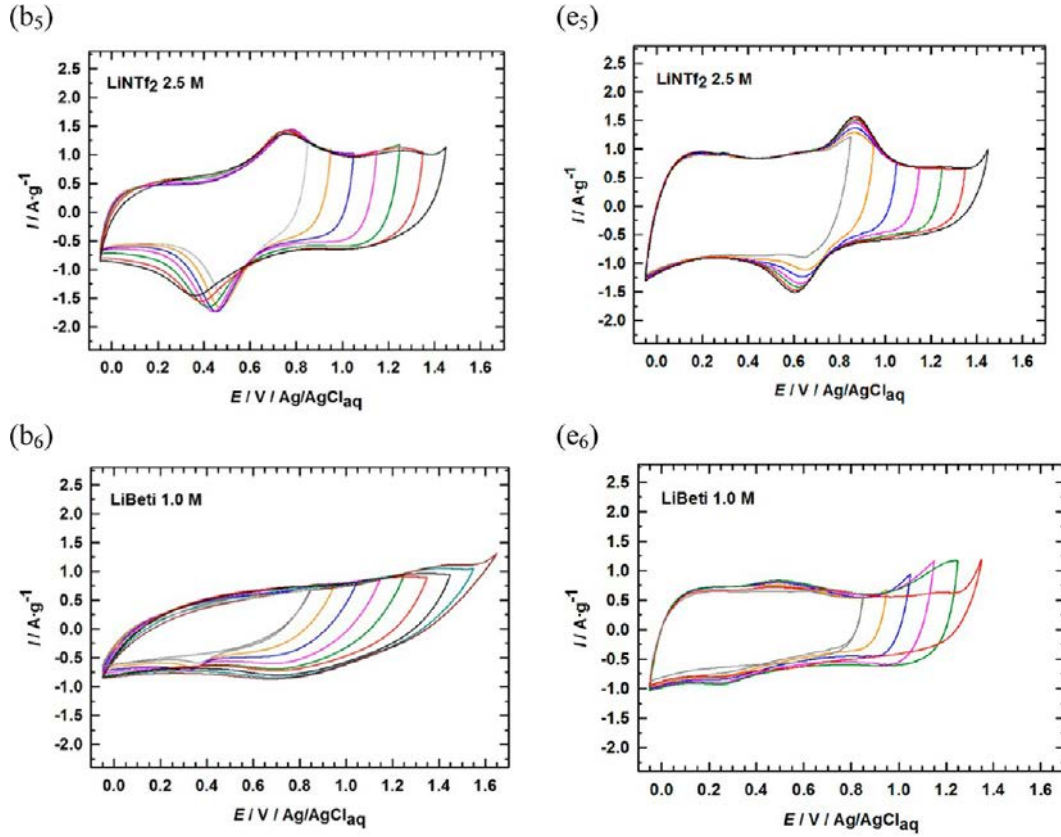


Figure 8. Comparative cyclic voltammograms of MnO₂ Birnessite (b_i) and Cryptomelane Erachem (e_i) in 2 M Li₂SO₄ (1); 5 mol·L⁻¹ LiNO₃ (2); 1.8 M LiClO₄ (3); 2.5 M LiCH₃CO₂ (4); 2.5 M LiTFSI (5); 1.0 M LiBetri (6), at 5 mV·s⁻¹.

Table 5. Performances of Birnessite and Cryptomelane MnO₂ Electrode in Aqueous Lithium Salt Electrolytes at Optimal Composition C_{cycling}: Specific Capacities, Energies, and Efficiencies for 300 Cycles

lithium salt	C (M)	electrode material	C (F·g ⁻¹) at ΔE = 0.9 V	C (F·g ⁻¹) at ΔE = 1.4 V	energy (J·g ⁻¹) at ΔE = 1.4 V	η ^a (%) at ΔE = 1.4 V
Li ₂ SO ₄	2.0	Birnessite	179	185	181	98
		Cryptomelane	162	163	163	100
LiNO ₃	5.0	Birnessite	146	151	148	98
		Cryptomelane	183	171	167	99
LiClO ₄	1.8	Birnessite	153	172	169	95
		Cryptomelane	173	153	155	99
LiCH ₃ CO ₂	2.5	Birnessite	133	153	129	99
		Cryptomelane	150	136	82	100
LiC ₇ H ₁₅ CO ₂	0.5	Birnessite	101	120 ^b	86	99
LiLact	1.8	Birnessite	124		136 ^b	30
LiCH ₃ SO ₃	3.4	Birnessite	161	165	172	99
		Cryptomelane	171	165	168	99
LiTFSI	2.5	Birnessite	161	164	161	99
		Cryptomelane	171	165	168	99
LiBetri	1.0	Birnessite	87	131	189 ^b	80
		Cryptomelane	112	115	112	96 ^b
LiBob	2.2	Birnessite	188	253	260	99

^aη (C/C₀) capacity retention after 300 cycles. ^bη at 1.2 V.

that, below this value, the volume is no longer a determining factor of the electrochemical properties of the Birnessite material.

The cyclability of the different electrolytes was also studied as a function of scan rate; for example, the CV curves for LiNO₃ and LiClO₄ were presented in Figure 11 and capacity values for all electrolytes are reported in Table 6. In the latter figure, the capacitance is seen to decrease initially but then increase as the cycle number increases. While these results are comparable to

the literature for similar materials,²² the cause of the increasing capacitance is not known with certainty; however, it most likely involves mechanical breakdown of the material, opening up the pores to expose a higher surface area to the electrolyte.

We show in Figure 11 that both LiNO₃ and LiClO₄ electrolytes allow maintenance of a good shape of CVs up to 50 mV·s⁻¹ (current densities of 10 A·g⁻¹), whereas a decrease in capacitance was observed when the scan rate increases in the

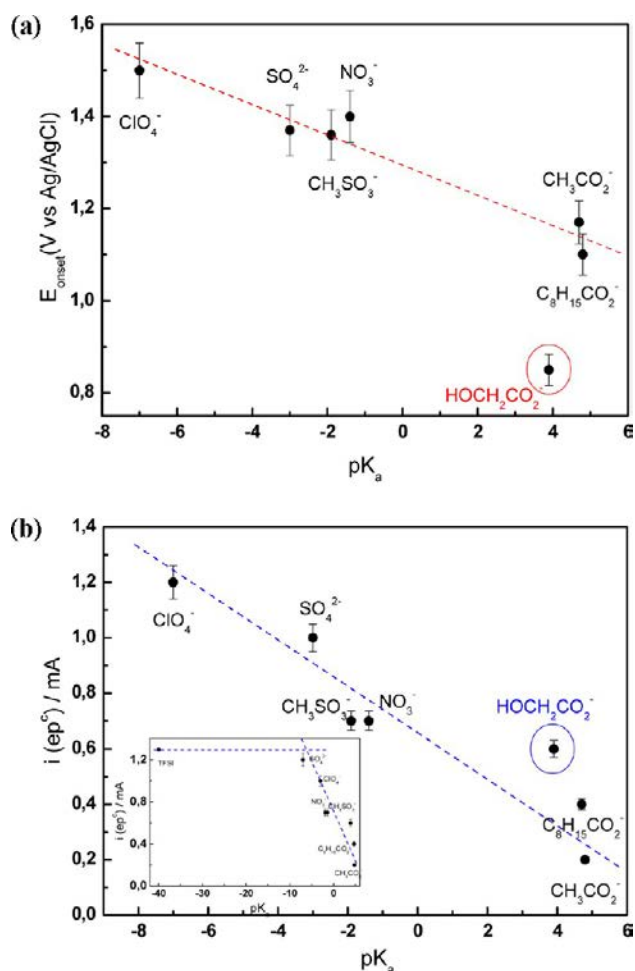


Figure 9. Variation of the potential limit (a) on oxidation, E_{onset} or (b) in reduction, expressed by $i(\text{ep}^c)$ as a function of the anion (denoted X^-) basicities expressed by their pK_a values (HX/X^-).

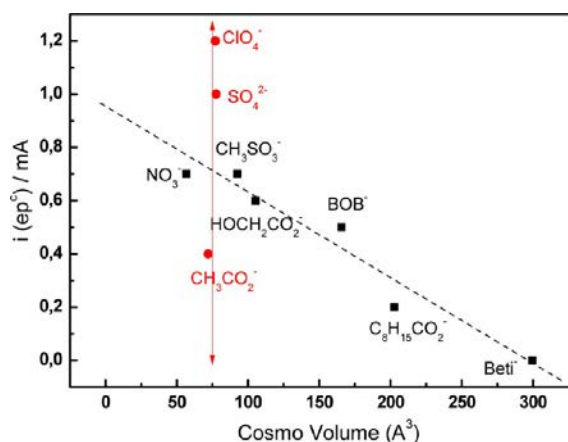


Figure 10. Variation of potential limit on reduction expressed by $i(\text{ep}^c)$ as a function of the Cosmo volume of the selected anions.

case of lithium methanesulfonate, lithium acetate, or lithium octanoate, as shown in Table 6.

As described by Ardizzone et al.,⁴⁵ at high sweep rates, the cation diffusion is limited to the more accessible sites, called the “outer surface of the electrode”. In our case, the important decrease of the capacitance suggests that the extrapolated value

at infinite sweep rate (corresponding to the “outer surface”) is very small.

This observation applies when comparing LiTFSI and Li_2SO_4 yet contrasts with diffusion of lithium ions in solution ($D = 2.9 \times 10^{-10} \text{ m}^2\cdot\text{s}^{-1}$ for LiTFSI and $D = 4.2 \times 10^{-10} \text{ m}^2\cdot\text{s}^{-1}$ for Li_2SO_4 measured by pulsed-field gradient spin-echo NMR), indicating a higher diffusion of lithium ions in the case of LiTFSI in water compared to Li_2SO_4 . In the inside of the Birnessite interlayer, lithium ions diffusion depends on the anions nature and their polarizability, which condition the lithium dissociation and cation solvation and, thus, the intercalation of cation solvated by water. This is in accordance with a pseudocapacitive mechanism of charge storage, arising from faradic reactions sensitive to diffusion phenomena of the electroactive species of electrolyte (Li^+ , Na^+ , H^+) into our bulk porous solid electrode material.



Comparable decreases have been observed for similar compounds used under analogous conditions.⁴⁴ Figure 12 shows that this effect is more important for the organic-containing electrolytes samples, especially those having carboxylate anion.

4. CONCLUSION

In this study, the comparison of performance of synthesized Birnessite-type and commercial Cryptomelane-type MnO_2 was investigated in ten neutral aqueous electrolytes for supercapacitor applications. The capacitances, energies, and efficiencies are calculated; results indicate clearly that electrolytes based on a mineral lithium salt under neutral conditions and high salt concentrations (up to 5 M) have better electrochemical performances than organic based anions, up to 1.4 V, with good material stability and capacity retention. The relationship between transport properties, electrostatic and steric hindrance considerations of hydrated ions, and their electrochemical performances is discussed to understand further the lithium intercalation-desintercalation processes in the lamellar or tunnel structure of investigated MnO_2 . Results show an evident correlation between the capacitive response of Birnessite and Cryptomelane observed by cyclic voltammetry and two key parameters: the basicity and the volume (described herein by using the COMO-RS methodology) of the anion in each investigate aqueous lithium salt electrolyte. It seems possible to charge and discharge electrode material at higher potential up to 1.6 V vs Ag/AgCl(aq) in neutral pH conditions. Moreover, CVs obtained in LiNO_3 , LiTFSI, Li_2SO_4 , and LiClO_4 illustrate the predominance of surface pseudocapacitive phenomena in the case of Cryptomelane, and the superimposed redox peaks are more pronounced by using Birnessite than Cryptomelane, especially for electrolytes based on a lithium salt composed of anions having low volumes and diameters lesser than the interlamellar space (i.d. $< 0.7 \text{ nm}$). Finally, the best favorable electrolytes based on LiNO_3 or on LiClO_4 salts allow maintainance of a good shape of CVs up to $50 \text{ mV}\cdot\text{s}^{-1}$ (current densities of $10 \text{ A}\cdot\text{g}^{-1}$), which is very promising for the progress of energy storage systems with environmentally friendly electrolytes and material.

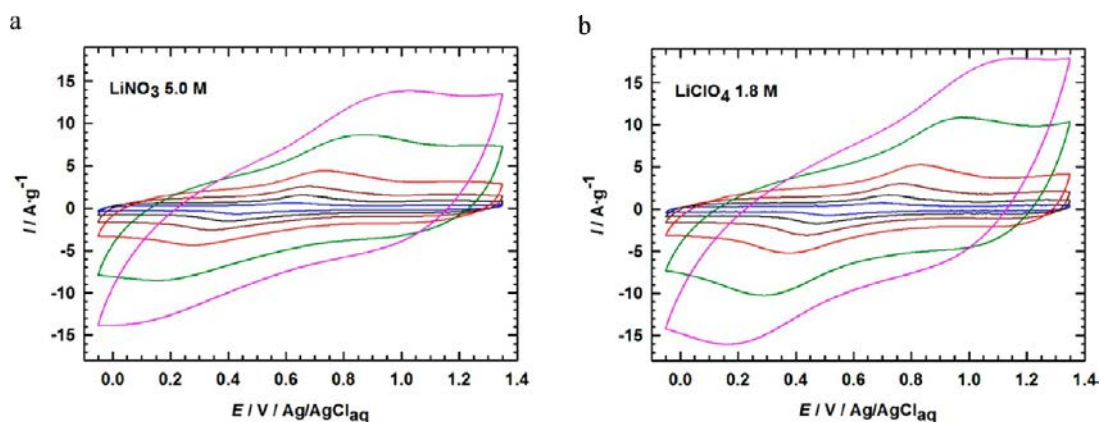


Figure 11. Cyclic voltammograms of MnO₂ (Birnessite) in aqueous 5 M LiNO₃ (a) and 1.8 M LiClO₄ (b) as a function of scan rate from 2 to 50 mV·s⁻¹.

Table 6. Specific Capacities of Birnessite-Type MnO₂ Electrode in Aqueous Electrolytes at Optimal Composition C_{cycling} as a Function of Cycling Scan Rate

electrode material	lithium salt	ΔE (V)	specific capacity at the following scan rate, ν (mV·s ⁻¹)				
			2	5	10	20	50
Birnessite	Li ₂ SO ₄	1.4	187	179	160	134	90
Cryptomelane		1.35	190	166	152	135	106
Birnessite	LiNO ₃	1.35	160	151	146	132	104
Cryptomelane		1.4	183	177	171	162	145
Birnessite	LiClO ₄	1.4	169	167	161	149	126
Cryptomelane			167	158	149	138	120
Birnessite	LiCH ₃ CO ₂	1.1	150	132	110	81	43
Cryptomelane			151	136	119	97	60
Birnessite	LiTFSI	1.2	176	161	138	109	69
Cryptomelane		1.4	180	171	156	139	120
Birnessite	LiBetri	0.9	123	92	64	38	16
Cryptomelane			124	112	98	81	52
Birnessite	LiOcta	1.1	140	113	83	58	31
Birnessite	LiCH ₃ SO ₃	1.35	173	160	139	106	62
Birnessite	LiBOB	0.9	252	190	152	117	66

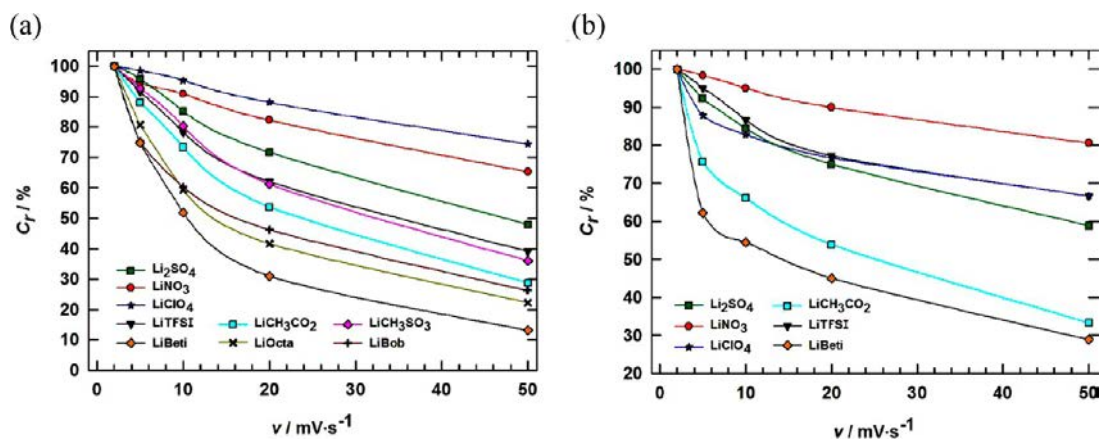


Figure 12. Relative specific capacities of Birnessite (a) and Cryptomelane (b) electrodes in aqueous electrolytes at C_{cycling} as a function of cycling scan rate.

AUTHOR INFORMATION

Corresponding Author

*E-mail: meriem.anouti@univ-tours.fr. Fax: (33)247367360. Tel: (33)247366951.

Notes

The authors declare no competing financial interest.

ACKNOWLEDGMENTS

This study is supported by the ADEME France and CEA Le Ripault (Ph.D. grant of A.B.).

REFERENCES

- (1) Davies, A.; Yu, A. Material Advancements in Supercapacitors: From Activated Carbon to Carbon Nanotube and Graphene. *Can. J. Chem. Eng.* **2011**, *89*, 1342–1357.
- (2) Lewandowski, A.; Olejniczak, A.; Galinski, M.; Stepniak, I. Performance of Carbon–Carbon Supercapacitors Based on Organic, Aqueous and Ionic Liquid Electrolytes. *J. Power Sources* **2010**, *195*, 5814–5819.
- (3) Zhang, Y.; Feng, H.; Wu, X.; Wang, L.; Zhang, A.; Xia, T.; Dong, H.; Li, X.; Zhang, L. Progress of Electrochemical Capacitor Electrode Materials: A Review. *Int. J. Hydrogen Energy* **2009**, *34*, 4889–4899.
- (4) Moser, F.; Athouël, L.; Crosnier, O.; Favier, F.; Bélanger, D.; Brousse, T. Transparent Electrochemical Capacitor Based on Electrodeposited MnO₂ Thin Film Electrodes and Gel-Type Electrolyte. *Electrochem. Commun.* **2009**, *11*, 1259–1261.
- (5) Xu, C.; Kang, F.; Li, B.; Du, H. Recent Progress on Manganese Dioxide Based Supercapacitors. *J. Mater. Res.* **2010**, *25*, 1421–1432.
- (6) Inoue, R.; Nakayama, M. Capacitive Behavior of Vertically Aligned Multilayered Manganese Oxide Film. *Meeting Abstracts* **2009**, MA2009–02, 3027.
- (7) Athouël, L.; Arcidiacono, P.; Ramirez-Castro, C.; Crosnier, O.; Hamel, C.; Dandeville, Y.; Guillemet, P.; Scudeller, Y.; Guay, D.; Bélanger, D.; et al. Investigation of Cavity Microelectrode Technique for Electrochemical Study with Manganese Dioxides. *Electrochim. Acta* **2012**, *86*, 268–276.
- (8) Guillemet, P.; Brousse, T.; Crosnier, O.; Dandeville, Y.; Athouël, L.; Scudeller, Y. Modeling Pseudo Capacitance of Manganese Dioxide. *Electrochim. Acta* **2012**, *67*, 41–49.
- (9) Mosqueda, H. A.; Crosnier, O.; Athouël, L.; Dandeville, Y.; Scudeller, Y.; Guillemet, P.; Schleich, D. M.; Brousse, T. Electrolytes for Hybrid Carbon-MnO₂ Electrochemical Capacitors. *Electrochim. Acta* **2010**, *55*, 7479–7483.
- (10) Mysyk, R.; Raymundo-Pinero, E.; Anouti, M.; Lemordant, D.; Béguin, F. Pseudo-Capacitance of Nanoporous Carbons in Pyrrolidinium-Based Protic Ionic Liquids. *Electrochem. Commun.* **2010**, *12*, 414–417.
- (11) Simon, P.; Gogotsi, Y. Charge Storage Mechanism in Nanoporous Carbons and Its Consequence for Electrical Double Layer Capacitors. *Philos. Trans. R. Soc., A* **2010**, *368*, 3457–3467.
- (12) Brousse, T.; Toupin, M.; Dugas, R.; Athouël, L.; Crosnier, O.; Bélanger, D. Crystalline MnO₂ as Possible Alternatives to Amorphous Compounds in Electrochemical Supercapacitors. *J. Electrochem. Soc.* **2006**, *12*, A2171–A2180.
- (13) Ab Manan, N.; Hardacre, C.; Jacquemin, J.; Rooney, D. W.; Youngs, T. G. A. Evaluation of Gas Solubility Prediction in Ionic Liquids Using COSMOthermX. *J. Chem. Eng. Data* **2009**, *54*, 2005–2022.
- (14) *Gaussian View 3.0*; Gaussian, I. S. Inc.: Pittsburgh, PA, 2000–2003.
- (15) Schaefer, A.; Huber, C.; Ahlrichs, R. Fully Optimized Contracted Gaussian Basis Sets of Triple Zeta Valence Quality for Atoms Li to Kr. *J. Chem. Phys.* **1994**, *100*, 5829–5835.
- (16) Ahlrichs, R. *TURBOMOLE User's Manual*, Version 5.7; COSMOlogic GmbH & Co. KG: Leverkusen, Germany, 2004.
- (17) Eckert, F.; Klamt, A. *COSMOlogic Version C2.1*; GmbH & Co. KG: Leverkusen, Germany, 2006.
- (18) Klamt, A.; Eckert, F. COSMO-RS: A Novel and Efficient Method for the a Priori Prediction of Thermophysical Data of Liquids. *Fluid Phase Equilib.* **2000**, *172*, 43–72.
- (19) Ching, S.; Krukowska, K. S.; Suib, S. L. A New Synthetic Route to Todorokite-Type Manganese Oxides. *Inorg. Chim. Acta* **1999**, *294*, 123–132.
- (20) David, B. *Mineralogy Database*; 2012; <http://webmineral.com/>.
- (21) Reddy, R. N.; Reddy, R. G. Synthesis and Electrochemical Characterization of Amorphous MnO₂ Electrochemical Capacitor Electrode Material. *J. Power Sources* **2004**, *132*, 315–320.
- (22) Athouël, L.; Moser, F.; Dugas, R.; Crosnier, O.; Bélanger, D.; Brousse, T. Variation of the MnO₂ Birnessite Structure upon Charge/Discharge in an Electrochemical Supercapacitor Electrode in Aqueous Na₂SO₄ Electrolyte. *J. Phys. Chem. C* **2008**, *112*, 7270–7277.
- (23) Toupin, M.; Brousse, T.; Bélanger, D. Charge Storage Mechanism of MnO₂ Electrode Used in Aqueous Electrochemical Capacitor. *Chem. Mater.* **2004**, *16*, 3184–3190.
- (24) Chen, Y. C.; Ouyang, C. Y.; Song, L. J.; Sun, Z. L. Electrical and Lithium Ion Dynamics in Three Main Components of Solid Electrolyte Interphase from Density Functional Theory Study. *J. Phys. Chem. C* **2011**, *115*, 7044–7049.
- (25) Celeda, J. On the Chemical Form of Sodium(+) Ion in Aqueous Solutions. *Collect. Czech. Chem. Commun.* **1983**, *48*, 1680–1694.
- (26) Gucker, F. T.; Stubble, D.; Hill, D. J. The Isentropic Compressibilities of Aqueous Solutions of Lithium Chloride at 298.15 K. *J. Chem. Thermodyn.* **1977**, *9*, 987–989.
- (27) Litvinenko, I. V. Compressibility of Aqueous Solutions of Electrolytes and Hydration of Anions and Cations. *Zh. Strukt. Khim.* **1963**, *4*, 830–836.
- (28) Rakos, M.; Tarabckova, E.; Varga, Z.; Tirpak, A. Anomalous Magnetic Properties of Aqueous LiCl Solutions. *Collect. Czech. Chem. Commun.* **1965**, *30*, 1989–1999.
- (29) Koch, V. R.; Dominey, L. A.; Nanjundiah, C.; Ondrechen, M. J. The Intrinsic Anodic Stability of Several Anions Comprising Solvent-Free Ionic Liquids. *J. Electrochem. Soc.* **1996**, *143*, 798–803.
- (30) Atkinson, G.; Hallada, C. J. The Conductance of Hexafluoroarsenic Acid and Its Lithium, Sodium, and Potassium Salts in Water at 25°. *J. Phys. Chem.* **1960**, *64*, 1487–1491.
- (31) Ue, M. Mobility and Ionic Association of Lithium and Quaternary Ammonium Salts in Propylene Carbonate and γ -Butyrolactone. *J. Electrochem. Soc.* **1994**, *141*, 3336–3342.
- (32) Salomon, M. Conductance of Solutions of Lithium Bis-(trifluoromethanesulfone)imide in Water, Propylene Carbonate, Acetonitrile and Methyl Formate at 25°C. *J. Solution Chem.* **1993**, *22*, 715–725.
- (33) Smirnov, P. R.; Trostin, V. N. Structure of the Nearest Surrounding of the Li⁺ Ion in Aqueous Solutions of Its Salts. *Russ. J. Gen. Chem.* **2006**, *76*, 175–182.
- (34) Brouillette, D.; Perron, G.; Desnoyers, J. E. Effect of Viscosity and Volume on the Specific Conductivity of Lithium Salts in Solvent Mixtures. *Electrochim. Acta* **1999**, *44*, 4721–4742.
- (35) Gernon, M. D.; Wu, M.; Buszta, T.; Janney, P. Environmental Benefits of Methanesulfonic Acid. Comparative Properties and Advantages. *Green Chem.* **1999**, *1*, 127–140.
- (36) Wolf, G.; Vacek, V.; Pekarek, V. Enthalpies of Solution and of Crystallization of Lithium Nitrate and of Lithium Nitrate Trihydrate in Water at 25°C. *J. Solution Chem.* **1990**, *19*, 1029–1239.
- (37) Stejskal, E. O.; Tanner, J. E. Spin Diffusion Measurements: Spin Echoes in the Presence of a Time-Dependent Field Gradient. *J. Chem. Phys.* **1965**, *42*, 288–292.
- (38) Ananikov, V. P. Characterization of Molecular Systems and Monitoring of Chemical Reactions in Ionic Liquids by Nuclear Magnetic Resonance Spectroscopy. *Chem. Rev. (Washington, DC, U. S.)* **2011**, *111*, 418–454.
- (39) Tanner, J. E. Use of the Stimulated Echo in NMR Diffusion Studies. *J. Chem. Phys.* **1970**, *52*, 2523–2526.
- (40) Cotts, R. M.; Hoch, M. J. R.; Sun, T.; Markert, J. T. Pulsed Field Gradient Stimulated Echo Methods for Improved NMR Diffusion Measurements in Heterogeneous Systems. *J. Magn. Reson.* **1989**, *83*, 252–266.
- (41) Brousse, T.; Taberna, P.-L.; Crosnier, O.; Dugas, R.; Guillemet, P.; Scudeller, Y.; Zhou, Y.; Favier, F.; Bélanger, D.; Simon, P. Long-Term Cycling Behavior of Asymmetric Activated Carbon/MnO₂ Aqueous Electrochemical Supercapacitor. *J. Power Sources* **2007**, *173*, 633–641.
- (42) Ghodbane, O.; Ataherian, F.; Wu, N.-L.; Favier, F. In Situ Crystallographic Investigations of Charge Storage Mechanisms in MnO₂-Based Electrochemical Capacitors. *J. Power Sources* **2012**, *206*, 454–462.
- (43) Levi, M. D.; Aurbach, D. Simultaneous Measurements and Modeling of the Electrochemical Impedance and the Cyclic

Voltammetric Characteristics of Graphite Electrodes Doped with Lithium. *J. Phys. Chem. B* **1997**, *101*, 4630–4640.

(44) Atribak, I.; Bueno-López, A.; García-García, A.; Navarro, P.; Frías, D.; Montes, M. Catalytic Activity for Soot Combustion of Birnessite and Cryptomelane. *Appl. Catal. B: Environ.* **2010**, *93*, 267–273.

(45) Ardizzone, S.; Fregonara, G.; Trasatti, S. “Inner” and “Outer” Active Surface of RuO₂ Electrodes. *Electrochim. Acta* **1990**, *35*, 263–267.